Support of Cd doping in SnO_2 nanoparticles to enhance its thermoelectric parameters

N. U. Rehman[a,*], A. Hussain[b], S. M. Ali[c,*], J. Ahmad[a], S. A. Buzdar[a], K. Mahmood[d], Z. A. Shah[e], S. D. Ali[f], M. A. Shar[g]

[a]*Institute of Physics, The Islamia University of Bahawalpur, Bahawalpur 63100, Pakistan*

[b]*Department of Physics, Khwaja Fareed University of Engineering and Information Technology, Rahim Yar Khan 64200, Pakistan*

[c]*Department of Physics and Astronomy, College of Science, P.O. BOX 2455, King Saud University, Riyadh 11451, Saudi Arabia*

[d]*Department of Physics, Government College University, Faisalabad, Pakistan*

[e]*Department of Physics, Allama Iqbal Open University, Islamabad, P. O. Box 44310, Pakistan*

[f]*Nanoscience and Technology Department, National Centre for physics, QAU campus, 45320, Islamabad, Pakistan*

[g]*Department of Mechanical & Energy Systems Engineering, Faculty of Engineering and Informatics, University of Bradford, Bradford BD7 1DP, UK*

In the present study we have successfully synthesized undoped and Cd doped SnO_2 nanoparticles using the Sol-gel method with different concentrations of Cd solutions, and Seebeck coefficient and electrical conductivity have been reported at various temperatures. The structural, morphological, thermoelectric and electrical properties of undoped and doped samples were by XRD, scanning electron microscopy, Raman spectroscopy, Seebeck effect and two point probe electrical measurement. XRD show the rutile tetragonal structure and the enhanced particle size in the range of 18.12 nm to 25.08 nm, and Raman active mode at 479cm^{-1}, 632cm^{-1} and 775cm^{-1} were measured by Raman spectroscopy. Morphology of the nanoparticles by using Scanning electron microscopy have revealed the random spherical shape and cluster formation of these nanoparticles. The maximum value of seebeck coefficient, electrical conductivity and power factor for 6% doped SnO_2 samples were found to be -297.92μV/°C, 33.33Ω^{-1}m^{-1} and 0.129117 x 10^6 Wm^{-1}/°C^2, respectively. These results reveal that the Cd doped tin dioxide (SnO_2) nanoparticles can be used as a good candidate for thermoelectric applications.

(Received September 16, 2023; Accepted November 16, 2023)

Keywords: Cd doped SnO_2, Nanoparticles, Thermoelectric properties, Seebeck coefficient

1. Introduction

In the present era, the scientific community is looking for alternative and reproducible energy sources which are becoming increasingly important to fulfill the energy requirements. In this context, thermoelectricity offers some interesting opportunities because of its capabilities to convert thermal energy to electrical energy and along with an additional benefit of having longer device life cycles. By using the thermoelectric sources, the conversion of large part of the waste heat might be possible to convert into electrical energy that is being added to our atmosphere. However, the choice and optimization of correct material with suitable thermoelectric properties and the design of the devise for the said purpose are very important to achieve the best conversion efficiency of the heat energy [1]. For a thermoelectric power generator the efficiency can be determined by a dimensionless parameter called figure of merit as given,

* Corresponding authors: naeem.rehman@iub.edu.pk
https://doi.org/10.15251/JOR.2023.196.653

$$ZT = \frac{S^2\sigma}{k_{tot}} \quad (1)$$

where S, σ, T and k_{tot} denotes the Seebeck coefficient, electrical conductivity, absolute temperature and total thermal conductivity respectively [2].The materials can be used in thermoelectric applications if they have high value of Seebeck coefficient and electrical conductivity and lower value of thermal conductivity. Researchers are trying to find the materials that have high figure of merit value [3].

There have been many materials that are proposed in order to harvest their thermoelectric behavior including Sb_2Te_3 [4], Bi_2Te_3 [4], PbTe [5], β – Zn_4Sb_3 [6]and clathrates [1] etc. In addition oxide semiconductor materials have also seeked attention of the researcher for their potential use in the energy conversion. Various oxide materials have already been reported for their thermoelectric properties like, Cu_2InO_4, $CuAlO_2$, and Zn_2GeO_4) [7].Among these, tin dioxide is a material with high electrical conductivity and optical transparency in the visible spectral region and also possess the potential to be used for thermoelectric power generations.Intrinsically being an n-type semiconductor material, tin dioxide (SnO_2) has a band gap in the range of 3.6eV to 4.3eV by the existence of intrinsic defects such as oxygen vacancies [2], [8], [9].

In recent times, many reports have been published related to the electrical or thermoelectric properties of tin oxide.Mohagheghi*et. al.* [10] and S. Yanagiya*et. al.* [2] demonstrated that tin dioxide based bulk ceramics can be used at high temperature for thermoelectric power generations. Morgan and Wright *et.al.* reported the thermoelectric properties of single crystal SnO_2 [2]. P.P.Pradyumnan*et.al.,* reported the effect of the Co doping in tin oxide on thermoelectric behavior of the material. Similarly, study of the Lee et al enlighten the effects of Al doping in the tin oxide and corresponding variation in the thermoelectric behavior [11]. Kim *et. al.,*have seen the same property by doping the oxide material with antimony [12].

Many researchers were trying to improve power factors and thermoelectric performances of materials by different ways; Lindsay & Parker. Have seen maximum improved thermoelectric performance, when CdO alloyed with MgO [13]. Gao, Wang, Liu, Zhai, et al. reported the effect of 0.01% Ni doped in CdO at 1000k, which revealed the best ZT = 0.43 value as compared to the other thermoelectric materials [14]. Gao, Wang, Liu, Zha, et al. have seen a maximum increased ZT value, when Ag alloyed with CdO [15]. Park et al. study showed an improved power factor of about $1.25*10^{-3}Wm^{-1}K^{-2}$ at 1073K, when adding SnO in Zn of sample $Zn_{o.99}Sn_{0.01}O$ [16]. Rubenis et al. trying to checked thermoelectric behavior of SnO_2 with changing Sb concentration and it was seen that a maximum improved ZT value, approximately equal to 0.06 at 1073k of $Sn_{0.99}Sb_{0.01}O_2$ sample [17]. Yanagiya et al. study showed a maximum improved power factor of $4.8*10^{-4}$ Wm^{-1} K^{-2} at 1060K, when Bi doped in SnO_2 [18]. Here in this our focus of research is on the doping of SnO2 with cadmium and to study its structural and thermos-electrical properties. The undoped and Cd doped SnO2 nanostructures have been synthesized by the sol gel method. The doping has been achieved by simply changing the ratio of the Cd precursor in the solution.

2. Experimental detail

In this work, undopedand Cadmium doped Tin dioxide (SnO_2) nanoparticles were synthesized by using the Sol-gel method. For the synthesis purpose, Tin (II) Chloride dehydrate ($SnCl_2.2H_2O$), Cadmium Chloride monohydrate ($CdCl.H_2O$), Ammonia (NH_3) Solution (27%) and deionized water were taken as starting constituents in reaction process. For Undoped Tin dioxide (SnO_2) nanoparticles we dissolved 4.513 g Tin (II) Chloride ($SnCl_2.2H_2O$) in deionized water and stirred by a magnetic stirrer in beaker at 400 rpm stirring speed by maintaining the solution temperature at 50°C. Then, 20ml of Ammonia solution was added drop wise during stirring. The resultant solution was stirred for one hour to form gel. The formed gel was dried in microwave oven at 80°C temperature. The obtained powder was washed 10 times with a mixture of ethanol and deionized water to remove the impurities. At the end the prepared nanoparticles was grinded and annealed at 600°C temperature in furnace for 2 hour to improve the crystallinity of the nanoparticles. The Cd doped nanostructures were also prepared by employing the same synthesis

route. For the doping of Cd in the SnO2 nanostructures, the ratio (0%, 2%, 4% and 6%) of the ($CdCl.H_2O$) to ($SnCl_2.2H_2O$) was varied.

The structural study was carried out by examining the nanostructures by Bruker D8 x-ray diffractometer equipped with CuKα radiations of 0.154 nm. Morphology has been studied by JEOL JSM-7001F Field Emission Scanning Electron Microscope. The Raman spectra were achieved by a confocal mapping system having an excitation source of 632.8 nm. Thermoelectric measurements were carried out by using a self-made system. The electrical conductivity values were recorded by Hall system (Ecopia).

3. Results and Discussions

In order to study the structural behavior of the synthesized SnO2 nanoparticles, X-ray diffractometer was employed. The X-ray diffraction patterns of all the samples are shown in figure-1. All the indexed peaks in the XRD pattern are very well matched with the standard XRD pattern of tin dioxide (JCPDS card number 41-1445).With this comparison, itis also confirmed that these nanoparticles possesses tetragonal tin dioxide structure. The value of peak position at angle 2theta are 26.62°, 33.94°, 37.88°, 51.80°, 54.79° and 57.87° can be related with the miller indices (110), (101), (200), (211), (220) and (002), respectively. Spectra illustrates the formation of single phase with no impurities or cadmium related phase in the XRD pattern whichexhibits the high purity of the samples. The absence of impurities peaks such as CdO exhibits that the cadmium acts as a substitutional dopant rather than interstitials.

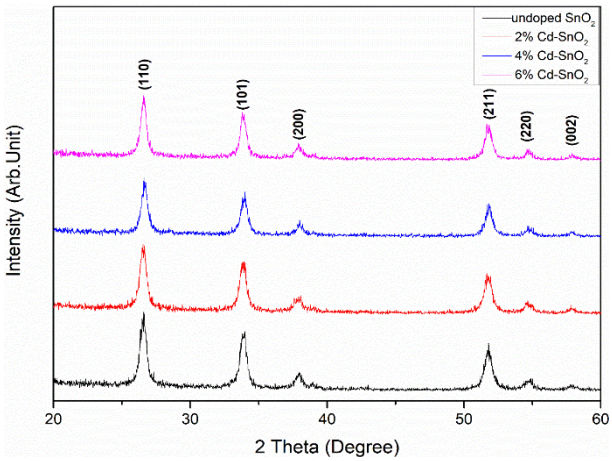

Fig. 1. X-Ray diffraction pattern for undoped and Cd doped SnO_2 nanoparticles.

The average crystallites size is calculated byusing the Scherrer formula after measuring the average peak broadening in the XRD spectra.

$$D = \frac{k\lambda}{\beta cos\theta} \tag{2}$$

where, D refers to average crystallite size, k denotes a Scherrer constant with value0.9.λrepresents the wavelength of X-ray source, β corresponds to the peak broadening and θ reflects theangle of diffraction.The average crystallites sizes D (nm) of undoped tin dioxide (SnO_2) nanoparticles are 18.13 nanometer. While its values for 2, 4 and 6%Cd-doped tin dioxide (SnO_2) nanoparticles are 20.27, 19.15 and 25.08 nanometers, respectively.

The value of the microstrain ε produced due to Cd dopinghas been calculated by using the following formula.

$$\varepsilon = \frac{\beta \cos\theta}{4} \quad (3)$$

and its value forundoped SnO_2 nanoparticles isfind to be $2.29x10^{-3}$ which exhibited a decreasing trend with the rise in the amount of Cd doping. The values for the average crystallite sizes and the microstrains are tabulated in table-1. The variation in the average crystallite sizes and microstrain valuesfor the synthesized SnO2 nanoparticles indicates towards the successful doping of Cd that effected the growth of the crystallites to grow in bigger sizes.

Table 1.Variation of crystallite size and microstrain of undoped and Cd doped tin dioxide (SnO_2) nanoparticles.

Undoped and Cadmium (Cd) doped Tin dioxide (SnO_2) Nanoparticles		
Samples	**Average Crystallites Size D (nm)**	**Average Micro-Strain ε**
Undoped SnO_2 Nanoparticles	18.12	0.00229
2%Cd-SnO_2 Nanoparticles	19.14	0.00225
4%Cd-SnO_2 Nanoparticles	20.26	0.00221
6%Cd-SnO_2 Nanoparticles	25.08	0.00201

SEM images for undoped and Cd doped SnO_2 nanoparticles have been shown in figure 3. The morphology of the synthesized SnO_2nanoparticles is seen to be uniform for all the samples e.g., spherical. Furthermore the size of the undoped and Cd doped nanoparticle is almost comparable in all the samples and measured to an average value of less than 25 nm. In addition, no agglomeration has been seen among the particles which are splendidly dispersed and maintained their individual identity.

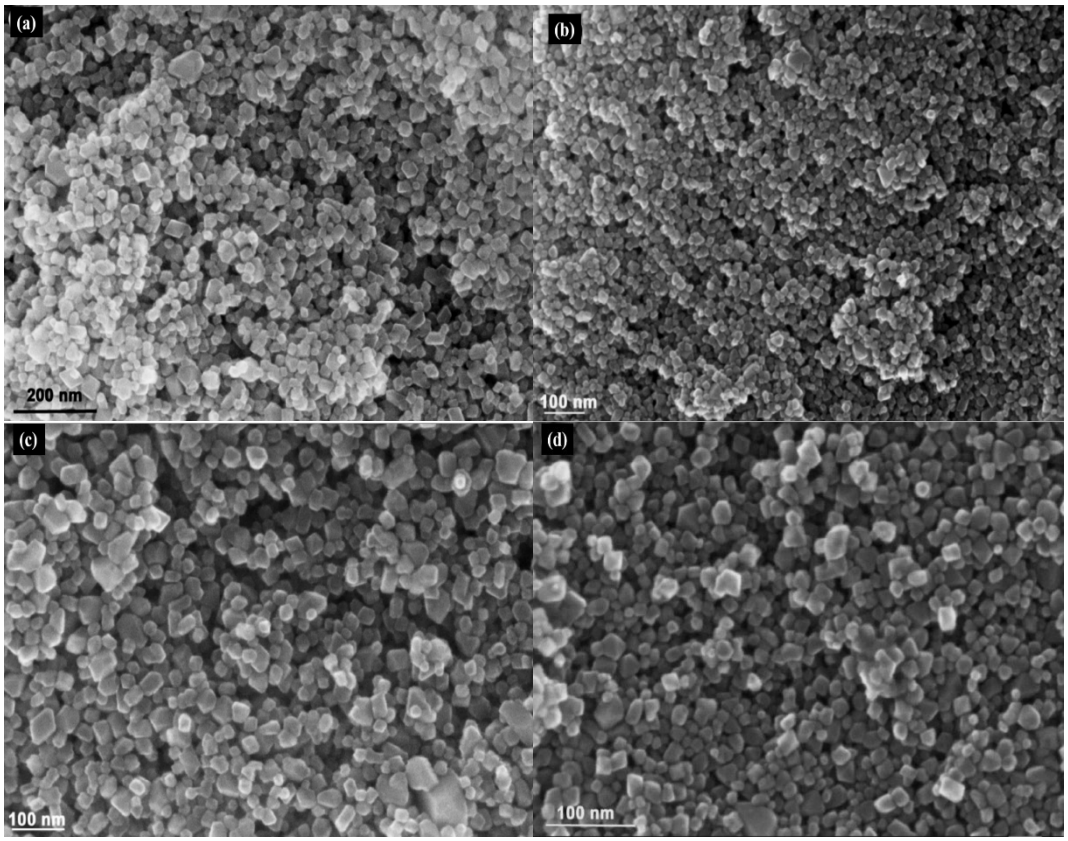

Fig. 2. (a) Undoped SnO_2 nanoparticles (b) 2%, (c) 4% and (d) 6% Cd doped SnO_2 nanoparticles.

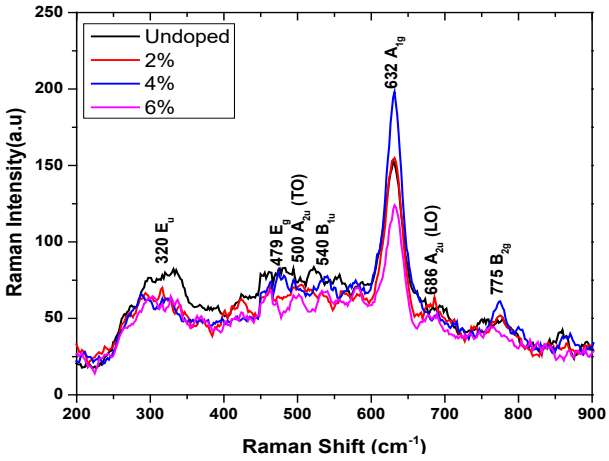

Fig. 3. Raman spectra of undoped and Cd doped SnO_2 nanoparticles.

The Raman spectra of Undoped and Cd-doped Tin dioxide (SnO_2) nanoparticles are shown in the figure 3. The Raman spectra of tin dioxide (SnO_2) and Cd-doped tin dioxide nanoparticles have properties of tetragonal rutile structure which is confirmed with X-Ray diffraction (XRD) outcomes. The spectra are determined in the range of 200 to 900 cm^{-1}. Raman spectroscopy characterization technique is a most common to find the vibration mode and phase of a material [19].

By using this technique, a normal mode of vibrations can be described like 3n where n denote the total quantity of atoms present in a primitive unit cell; also the coordinates provide the nearest value of displacement of the atoms as of their particular equilibrium position. By using group theory it is described that tin dioxide in its rutile phase make the 18 branches in the 1stBrillouin zone for vibration modes and the normal mode having mechanical description at the center of the first Brillouin zone is defined as [20]:

$$\Gamma = \Gamma^{+}_{1}(1A_{1g}) + \Gamma^{+}_{2}(1A_{2g}) + \Gamma^{+}_{3}(1B_{1g}) + \Gamma^{+}_{4}(1B_{2g}) + \Gamma^{-}_{5}(1E_{g}) + 2\Gamma^{-}_{1}(1A_{2u}) + 2\Gamma^{-}_{4}(B_{1u}) + 4\Gamma^{+}_{5}(E_{u})$$

Where the above terms can be described as, two modes are infrared (IR) active modes such as A_{2u} (single) and E_u (triply degenerated). In A_{2u} vibrations mode have one acoustic and one optic mode, while E_u modes have two acoustic and one optic mode. Four modes are Raman active that consist of three non-degenerated modes such as A_{1g}, B_{1g} and B_{2g}, two silent modes such as A_{2g} and B_{1u} one mode is doubly degenerated (E_g).

Tin Sn atom is at rest position while the Oxygen (O) atoms vibrate, a Raman active mode happens this time. While three modes are non-degenerated such as A_{1g}, B_{1g} and B_{2g} that vibrates perpendicular to the c-axis, one doubly degenerated (E_g) mode is vibrating the c-axis direction.

During the c-axis the rotating of oxygen (O) atom, along with each and every atom among six oxygen (O) atoms of octahedral receiving concerned within vibration provides a grow to the B_{1g} mode. Within IR active mode like A_{2g}, tin and oxygen atoms vibrate along the direction of c-axis, while within E_u mode tin and oxygen atoms vibrating in perpendicular direction to the c-axis. The mode such as B_{1u} are silent modes related to the vibrations of tin and oxygen atoms in the direction of the c-axis, while (A_{2g}) are to the vibration perpendicular to the c-axis plane[21].

A broad peak from 230 to 380cm^{-1} is related to the Eu mode, which exhibits the nanocrystalline structure of the samples [22], [23]. The peak at position 479cm^{-1} is related to Eg mode, and it is analogous to the vibration of oxygen in oxygen plane [22], [24].The observed Raman peaks at positions 632cm^{-1} and 775cm^{-1} related to A_{1g} and B_{2g}, respectively, and both modes are associated to the expansion and contraction of Sn-O bonds [24], [25]. The varying the intensity of these both peaks by increasing Cd content in the tin dioxide lattice may be owing to increasing grain size. The reason is that the modes A_{1g} and B_{2g} are sensitive to the grain size [22], [24]. The Raman bands at 500 cm^{-1} is a additional weak band while 686 cm^{-1} are related with A_{2u}

(LO) and A_{2u} (TO) modes; both are Infrared active modes, while the Raman forbidden B_{1u} mode at position 540 cm^{-1} [19].

These response can be related to the fact that the Cd replacing O in the Sn-O bonds modifying the local disorder and defects distribution, enhancing the growth of tin dioxide nanoparticles [23], [25]–[27], and this confirmed by XRD. This implies that the result gives a good insight into the effects of oxygen vacancies on the Raman response in SnO_2 nanostructure particles synthesized by using the Sol-gel techniques.

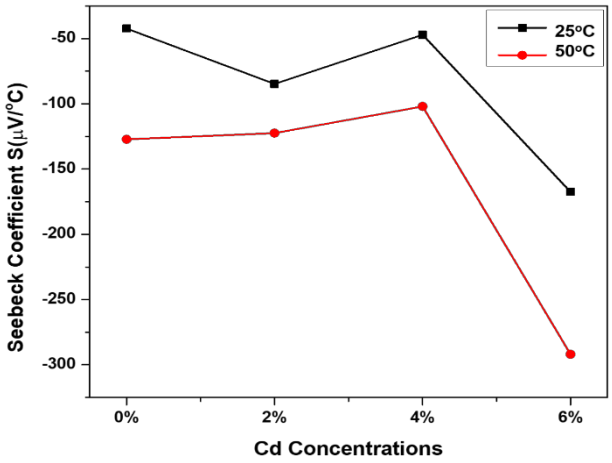

Fig. 4.Seebeck coefficient for undoped and Cd doped SnO_2 nanoparticles.

The variation in Seebeck Coefficient with various doping concentration of Cadmium in tin dioxide for temperatures on 25°C and 50°C for undoped and Cd-doped tin dioxide (SnO_2) nanoparticles are shown in figure 4.Seebeck coefficient at these temperatures is plotted as a function of Cd dopant. It can be seen that the value of seebeck coefficient reached to its maximum value (-297 μV/°C) for the highest doping level ~ 6%. For the lower values of Cd dopant it almost remain on the same level.

As the temperature rises the Seebeck coefficient of the all samples enhanced due to increase the number of charge carriers that reduced the Fermi energy level [28]. The negative values of Seebeck coefficient exhibits that the most of the charge carriers are electrons. Increase in the Cadmium ions concentrations in SnO_2 enhanced the induced voltage value produced within the samples materials.

Since the Cd^{2+} ions acts like an acceptor in tin dioxide lattice it will produce an acceptor energy levels close to the valence band. The electrons will move from the valence band to acceptor energy level with the creation of holes in the valence band that are accountable for the generation of induced emf. When the concentration of cadmium ions increase, large amount of electrons will leave the valence band and thereby raise the induced emf. The value of seebeck coefficient gets a value as large as -297μV/°C at 50 °C, for 6% concentrations of Cadmium doping in tin dioxide [2].

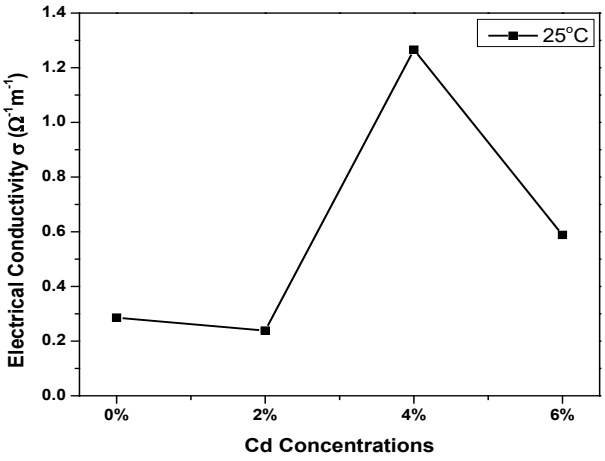

Fig. 5. Electrical Conductivity at temperature 25°C.

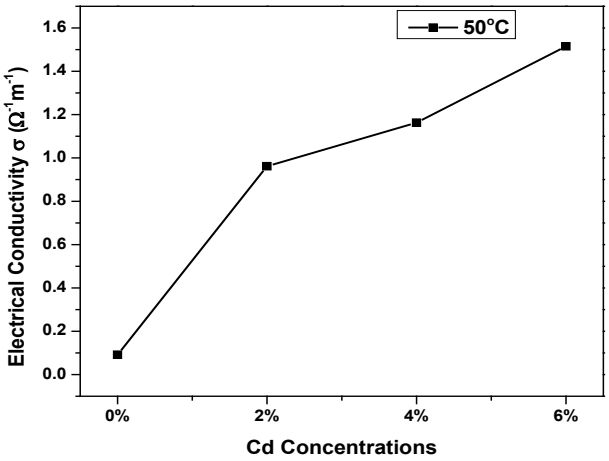

Fig. 6. Electrical Conductivity at temperature 50°C.

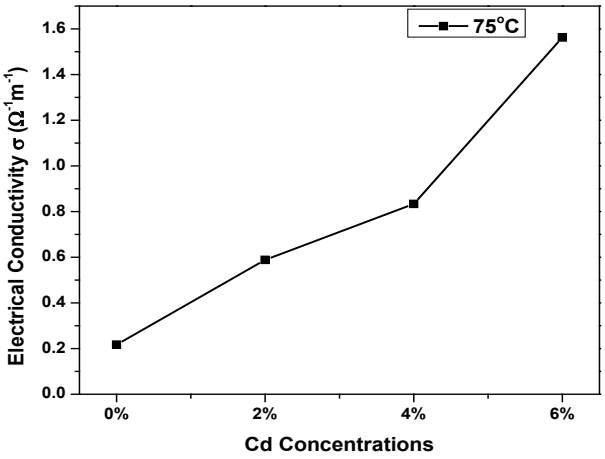

Fig. 7. Electrical Conductivity at temperature 75°C.

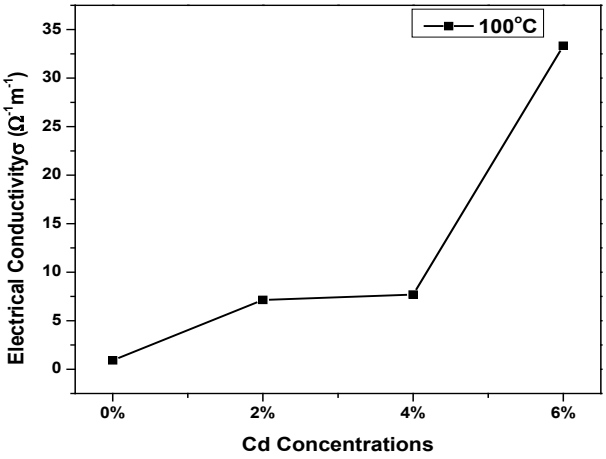

Fig. 8. Electrical Conductivity at temperature 100°C.

Temperature dependence electrical conductivity of undoped SnO_2 and Cd-doped SnO_2 with various concentration of cadmium (Cd) is investigated by using the two probe method. The temperature dependent electrical conductivity of undoped and Cd-doped SnO_2 nanoparticles is shown in figures 5, 6, 7 and 8.

For the undoped tin dioxide (SnO_2) nanoparticles the electrical conductivity enhanced by increasing temperature. Cadmium (Cd) doping increase the electrical conductivity, this representing that Cd doping produced free electrons in the conduction band. For undoped SnO_2 nanoparticles ,the electrical conductivity increased by increasing the temperature and reached a maximum value 0.91 $\Omega^{-1}m^{-1}$ at the temperature around 100°C. It is very attractive that the conductivity of 6% Cd-doped SnO_2 nanoparticles is highest value 33.33 $\Omega^{-1}m^{-1}$ then the other samples at high temperature. The response of electrical conductivity for the samples with different doping concentrations of can be described as the Cd doping with tin dioxide (SnO_2) nanoparticles increase the carrier mobility due to this the electrical conductivity increased[18].

Power factor is calculated as a function of seebeck coefficient and temperature dependent electrical conductivity.

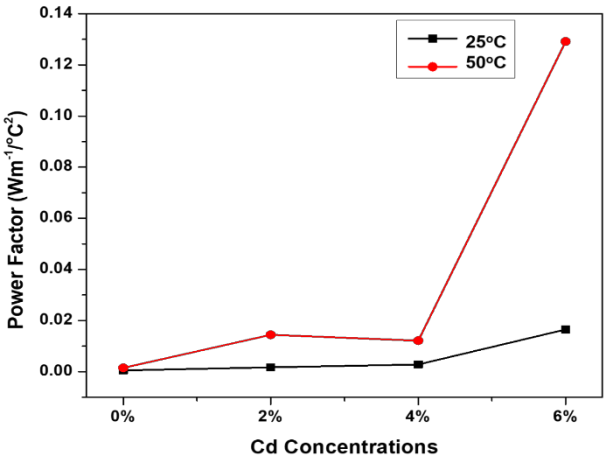

Fig. 9. Power factor for undoped and Cd doped SnO_2 nanoparticles.

The relation for power factor is given below

$$P = S^2\sigma \tag{4}$$

The graph between power factor at different temperatures values as shown in figure 11. It is observed from the graph is that the value of power factor is high for 6% Cd-doped Tin dioxide (SnO_2). It is also found that the value of power factor increase by increasing temperature. it is confirms from the power factor graph that Cd-doping can be choosing like an efficient way of tuning thermoelectric properties at high temperature [29].

4. Conclusion

The undoped and Cadmium (Cd) doped tin dioxide (SnO_2) nanoparticles have been successfully prepared by using Sol-gel technique with various concentrations of Cd solutions (0%, 2%, 4% and 6%). The formed nanoparticles had a tetragonal structure and the increase in the Cd concentration resulted in the rise of the crystallite size. The nanoparticles formed here possess random sized spherical shape and found in cluster form. Based on the thermal analysis, Cd doped SnO_2 nanoparticles are considered as the potential candidate for thermoelectric applications because of its high value of Seebeck Coefficient and electrical conductivity. The 6% Cd doped SnO_2 nanoparticles exhibits a maximum value of power factor at 50°C. These results make Cd doped tin dioxide nanoparticles to be an efficient candidate for thermoelectric applications.

Acknowledgments

The authors would like to extend their sincere appreciation to the Researcher supporting program at King Saud University, Riyadh, for funding this work under project number (RSPD2023R699).

References

[1] Gs. Nolas, J. L. Cohn, G. A. Slack, S. B. Schujman, Appl. Phys. Lett., vol. 73, no. 2, pp. 178-180, 1998; https://doi.org/10.1063/1.121747

[2] P. P. Pradyumnan, A. Paulson, M. S. NA, Cobalt doped SnO2: A new material for thermoelectric application, 2018.

[3] A. Rehman et al., Ceram. Int., vol. 45, no. 13, pp. 16275-16278, 2019; https://doi.org/10.1016/j.ceramint.2019.05.152

[4] H. Scherrer, S. Scherrer, Thermoelectr. Handb. Macro Nano, pp. 27-12, 2006; https://doi.org/10.1201/9781420038903.ch27

[5] Z. H. Dughaish, Phys. B Condens. Matter, vol. 322, no. 1-2, pp. 205-223, 2002; https://doi.org/10.1016/S0921-4526(02)01187-0

[6] T. Caillat, J.-P. Fleurial, A. Borshchevsky, J. Phys. Chem. Solids, vol. 58, no. 7, pp. 1119-1125, 1997; https://doi.org/10.1016/S0022-3697(96)00228-4

[7] S. Sivasankaran, P. K. Nayak, E. Günay, Solid State PhysicsMetastable, Spintronics Materials and Mechanics of Deformable Bodies: Recent Progress, 2020.

[8] D. Choi, J.-S. Park, Surf. Coat. Technol., vol. 259, pp. 238-243, 2014; https://doi.org/10.1016/j.surfcoat.2014.02.012

[9] D. Choi, W. J. Maeng, J.-S. Park, Appl. Surf. Sci., vol. 313, pp. 585-590, 2014; https://doi.org/10.1016/j.apsusc.2014.06.027

[10] M.-M. Bagheri-Mohagheghi, M. Shokooh-Saremi, Phys. B Condens. Matter, vol. 405, no. 19, pp. 4205-4210, 2010; https://doi.org/10.1016/j.physb.2010.06.067

[11] S.-H. Lee, J.-M. Choi, J.-H. Lim, J. Park, J.-S. Park, Ceram. Int., vol. 44, no. 2, pp. 1978-1983, 2018; https://doi.org/10.1016/j.ceramint.2017.10.141

[12] D. Kim, J. Park, J. H. Kim, Y.-C. Kang, H. S. Kim, Thin Solid Films, vol. 646, pp. 92-97, 2018; https://doi.org/10.1016/j.tsf.2017.11.036

[13] L. Lindsay, D. S. Parker, Phys. Rev. B, vol. 92, no. 14, p. 144301, 2015; https://doi.org/10.1103/PhysRevB.92.144301
[14] L. Gao et al., J. Alloys Compd., vol. 662, pp. 213-219, 2016; https://doi.org/10.1016/j.jallcom.2015.12.043
[15] L. Gao et al., Dalton Trans., vol. 45, no. 30, pp. 12215-12220, 2016; https://doi.org/10.1039/C6DT02348G
[16] K. Park, J. K. Seong, Y. Kwon, S. Nahm, W.-S. Cho, Mater. Res. Bull., vol. 43, no. 1, pp. 54-61, 2008; https://doi.org/10.1016/j.materresbull.2007.02.018
[17] K. Rubenis, S. Populoh, P. Thiel, S. Yoon, U. Müller, J. Locs, J. Alloys Compd., vol. 692, pp. 515-521, 2017; https://doi.org/10.1016/j.jallcom.2016.09.062
[18] S. Yanagiya, N. V. Nong, M. Sonne, N. Pryds, AIP Conference Proceedings, 2012, vol. 1449, no. 1, pp. 327-330; https://doi.org/10.1063/1.4731563
[19] S. Mehraj, M. S. Ansari, Thin Solid Films, vol. 589, pp. 57-65, 2015; https://doi.org/10.1016/j.tsf.2015.04.065
[20] M. Batzill, U. Diebold, Prog. Surf. Sci., vol. 79, no. 2-4, pp. 47-154, 2005; https://doi.org/10.1016/j.progsurf.2005.09.002
[21] M. Batzill, U. Diebold, Prog. Surf. Sci., vol. 79, no. 2-4, pp. 47-154, 2005; https://doi.org/10.1016/j.progsurf.2005.09.002
[22] V. Kumar et al., Mater. Res. Bull., vol. 85, pp. 202-208, 2017; https://doi.org/10.1016/j.materresbull.2016.09.020
[23] L. Z. Liu, X. L. Wu, J. Q. Xu, T. H. Li, J. C. Shen, P. K. Chu, Appl. Phys. Lett., vol. 100, no. 12, p. 121903, 2012; https://doi.org/10.1063/1.3696044
[24] A. S. Ahmed, M. L. Singla, S. Tabassum, A. H. Naqvi, A. Azam, J. Lumin., vol. 131, no. 1, pp. 1-6, 2011; https://doi.org/10.1016/j.jlumin.2010.07.017
[25] F. Gao et al., J. Alloys Compd., vol. 703, pp. 354-360, 2017; https://doi.org/10.1016/j.jallcom.2017.01.303
[26] L. Z. Liu, X. L. Wu, F. Gao, J. C. Shen, T. H. Li, P. K. Chu, Solid State Commun., vol. 151, no. 11, pp. 811-814, 2011; https://doi.org/10.1016/j.ssc.2011.03.029
[27] A. Kar, S. Kundu, A. Patra, J. Phys. Chem. C, vol. 115, no. 1, pp. 118-124, 2011; https://doi.org/10.1021/jp110313b
[28] F. J. DiSalvo, Science, vol. 285, no. 5428, pp. 703-706, 1999; https://doi.org/10.1126/science.285.5428.703
[29] A. Paulson, N. M. Sabeer, P. P. Pradyumnan, Mater. Res. Express, vol. 5, no. 4, p. 045511, 2018; https://doi.org/10.1088/2053-1591/aabd64